

Excitonic condensation in $\text{Pr}_{0.5}\text{Ca}_{0.5}\text{CoO}_3$

Jan Kuneš^{1*} and Pavel Augustinský¹

¹*Institute of Physics, Academy of Sciences of the Czech Republic,
Čukrovarnická 10, 162 53 Praha 6, Czech Republic*

(Dated: May 7, 2014)

Spontaneous second-order phase transitions are the hallmark of collective behavior in systems of interacting electrons. The notion of 'hidden order' was introduced for phases with distinct transport or thermodynamic properties, but without a clear, experimentally detected, order parameter typically in the form of modulation of the spin or charge density. The transition observed in the materials from the $(\text{Pr}_{1-y}\text{R}_y)_x\text{Ca}_{1-x}\text{CoO}_3$ ($\text{R}=\text{Nd}, \text{Sm}, \text{Eu}, \text{Gd}, \text{Tb}, \text{Y}$) family (PCCO) a decade ago, accompanied by a change from a metal to an insulator and a drop of the magnetic susceptibility, fulfills the above definition. Recently, the observation of an exchange splitting on the Pr site in materials lacking magnetic order added to the PCCO puzzle. Here, we address the physics of PCCO with dynamical mean-field model calculations and material specific calculations using the density-functional LDA+U method. We show that a condensation of spin-triplet, atomic-size excitons provides a consistent explanation of the observed physics and suggest that PCCO are the first known realization of this type of excitonic condensation, which was predicted to take place in the proximity of spin-state transitions.

The $\text{R}_x\text{A}_{1-x}\text{CoO}_3$ ($\text{R}=\text{La}, \dots$, and $\text{A}=\text{Ca}, \text{Sr}, \text{Ba}$) series exhibits a variety of phenomena including thermally and doping driven spin-state crossover, metal-insulator crossover, magnetic ordering or nanoscopic inhomogeneities. The root cause of the rich physics are quasi-degenerate Co $3d$ atomic multiplets and their interaction with the crystal lattice or doped charge carriers. The $(\text{Pr}_{1-y}\text{R}_y)_x\text{Ca}_{1-x}\text{CoO}_3$ ($\text{R}=\text{Nd}, \text{Sm}, \text{Eu}, \text{Gd}, \text{Tb}, \text{Y}$) family is unique among the cobaltites. A decade ago, Tsubouchi *et al.*^{1,2} observed a metal-insulator transition in $\text{Pr}_{0.5}\text{Ca}_{0.5}\text{CoO}_3$ associated with a drop of magnetic susceptibility and a sharp peak in the specific heat indicating the collective nature of the transition. Subsequently, the transition was observed in other PCCO materials with x and y in the ranges 0.2-0.5 and 0-0.3, respectively.³⁻⁵ Despite the evidence for a continuous, or very weakly first order, phase transition and the experimental effort⁶ no long-range order could be identified. The PCCO materials in this respect resemble the much famous hidden order prototype URu_2Si_2 ⁷. An important step towards understanding of the transition in PCCO was made by observation of $\text{Pr}^{3+} \rightarrow \text{Pr}^{4+}$ valence transition which take place simultaneously.⁸ Another clue to the nature of the PCCO hidden order is the exchange splitting of the Pr^{4+} Kramers ground state in the absence of ordered magnetic moments.^{4,6,9}

The basic features to be captured by a theory of the PCCO hidden order are: i) substantial

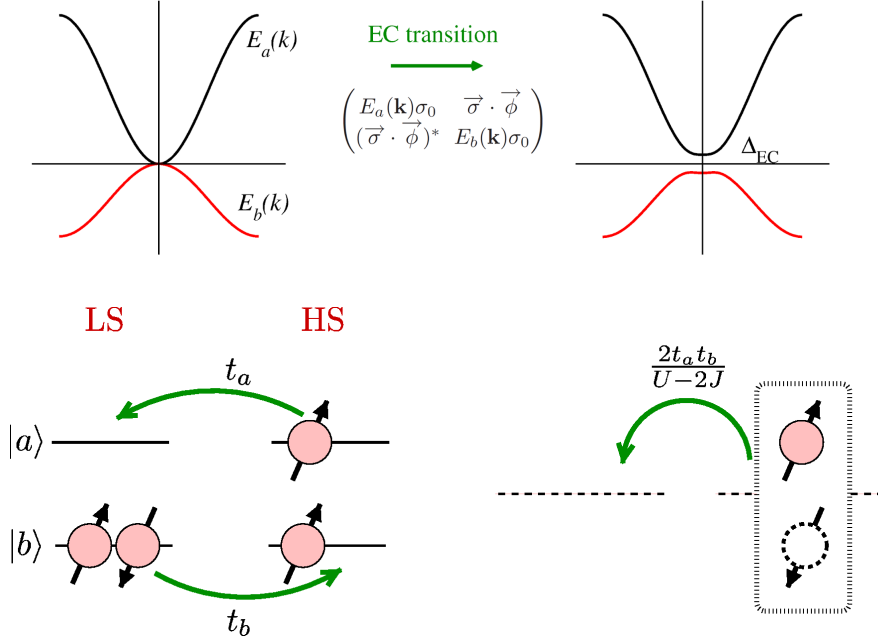


FIG. 1: Top, the weak-coupling view of the EC transition as opening of a gap due to a term in the mean-field Hamiltonian, which breaks the spin rotational symmetry. The σ_0 and $\vec{\sigma}$ are the unit and Pauli matrices in the 2×2 spin space. Bottom, the strong coupling low-energy limit of the present model with HS viewed as $S = 1$ bosons excited out of the LS vacuum. The bosons can propagate on the lattice by the depicted mechanism. The EC transition amounts to their Bose-Einstein condensation.

increase of resistivity below T_c , ii) the sharp peak in the specific heat at T_c , iii) the drop of the magnetic susceptibility and the departure from the Curie-Weiss behavior of the Co moments below T_c , iv) the Pr valence transition, v) the exchange splitting of the Pr^{4+} Kramers doublet in the absence of ordered magnetic moments. More subtle effects include the increase of T_c with pressure³, the lattice response consisting primarily in reduction of the Co-O-Co angle below T_c ³, and the apparent softness of the exchange field on Pr and the lack of a clear x-ray signature of the spin-state transition.^{6,10}

Motivated by our recent observation of excitonic instability in systems close to the spin-state transition¹¹, we have performed two types of investigations. First, we have studied the proposed excitonic condensation in the two-band Hubbard model and calculated the evolution of the relevant physical observables with temperature T . Second, we have performed $T = 0$ density-functional LDA+U¹² calculations for real materials and searched for stable solutions with EC order.

I. MODEL RESULTS

A minimal model to describe the spin-state transition material must capture the competition of the high-spin (HS) and low-spin (LS) states and propagation of electrons on the lattice. We have used a Hubbard model with two-orbital atoms on a bipartite lattice, see the Methods section for details. The nearest-neighbor hopping between orbitals of the same flavor was considered, which gives rise to a non-interacting bandstructure of Fig. 1 mimicking the e_g and t_{2g} bands in the perovskite structure. The crystal-field splitting was chosen so that the energy cost of creating a HS site in otherwise LS lattice is of the order of thermal energy $k_B T$. The same or similar model was previously studied in the context of the spin-state and metal-insulator transitions^{13,14}. Recent linear response calculations¹¹ revealed that at low temperature the system is unstable towards EC.¹⁵

The appearance of excitonic condensate (EC) in the model can be characterized by an orbital off-diagonal vector order parameter $\phi_i = \sum_{\alpha\alpha'=\uparrow,\downarrow} \sigma_{\alpha\alpha'} \langle a_{i\alpha}^\dagger b_{i\alpha'} \rangle$, where i is the site index and σ are the Pauli matrices. The model was chosen such that it leads to a ferro-EC order and so we drop the site index of ϕ_i from now on. In absence of an external electromagnetic field, there is a formal equivalence of the EC phase to s-wave spin-triplet superconductor consisting in replacing Cooper pairs by neutral excitons. S-wave, because the local order parameter ϕ is constant in the reciprocal space, and spin-triplet, because the Hund's coupling favors (S=1) HS states over their singlet counterparts. While superconducting pairing arises from higher-order processes and thus is weak, often with a complicated non-local structure, the excitonic pairing comes from the electron-hole attraction present in the bare interaction Hamiltonian (U-2J in the present model) and thus is strong and local. This leads to a high transition temperature T_c and a pairing that combines different orbital flavors, allowing a local spin-triplet order. In the weak coupling BCS limit the EC transition is a Fermi surface instability, while in the strong-coupling limit it can be viewed as a Bose-Einstein condensation of hard-core bosons^{11,16}, as shown in Fig. 1.

In the following, we study the behavior of various observables across T_c . With the density-density interaction used in the present model the vector ϕ is constrained to the xy -plane where it forms S_1 continuum of degenerate states.²⁸

First, we report results obtained with the particle density fixed to 2 electrons per atom. In Fig. 2 we show the evolution of the order parameter $|\phi|$. Finite ϕ below T_c is connected to appearance of the corresponding off-diagonal element in the local self-energy (shown in the Supplementary Figure

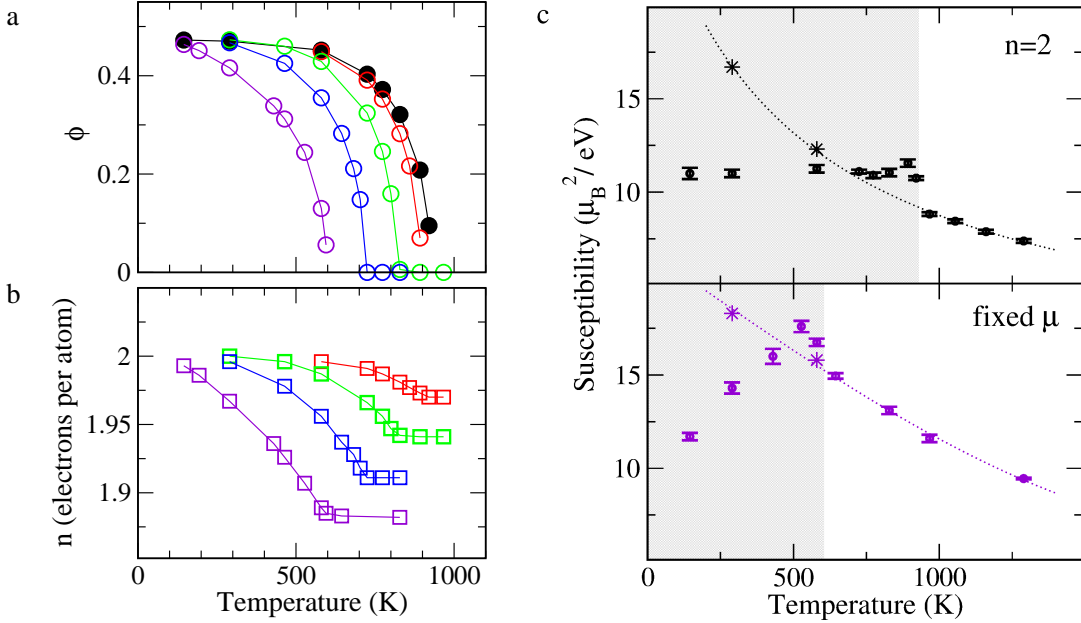


FIG. 2: (a) The order parameter $\phi = \langle a_{\uparrow}^{\dagger} b_{\downarrow} + a_{\downarrow}^{\dagger} b_{\uparrow} \rangle$ as a function of temperature for stoichiometric filling $n = 2$ (black) and at fixed chemical potential corresponding to hole doping between 0.03 and 0.12 (red to violet) in the normal phase. (b) Number of electrons per atom at fixed chemical potential across T_c (the same color coding as in (a)). (c) Top, the magnetic susceptibility χ as a function of temperature at the stoichiometric filling (circles with error bars). The dotted line shows $\chi(T)$ in the normal phase. The stars correspond to solutions below T_c constrained to the normal phase. The shaded area marks the EC phase. Bottom, the same as above in the system with fixed chemical potential and hole doping of 0.12 in the normal phase.

1), which leads to opening of a gap in the one-particle spectral density, as shown in Fig. 3. Opening of a gap naturally affects the optical conductivity shown in Fig. 3. Below T_c , the Drude peak is rapidly destroyed, as the spectral weight is pushed to higher frequencies, and the dc resistivity grows exponentially. The spin susceptibility $\chi_S(T)$, Fig. 2, changes from the Curie-Weiss behavior above T_c , reflecting the presence of thermally excited HS states, to a T -independent van Vleck paramagnetism arising from the on-site hybridization between LS and HS states represented by the off-diagonal self-energy. This effect is quite different from the spin-state transition characterized by vanishing of the HS population, which can be detected by x-ray absorption. In the EC phase the HS state remains populated and so the x-ray signature of the spin-state transition is missing. The sign of the χ_S jump at T_c depends on details of the system. In Fig. 2 we demonstrate that when T_c is reduced by doping χ_S is reduced below T_c . The results so far show that excitonic condensation

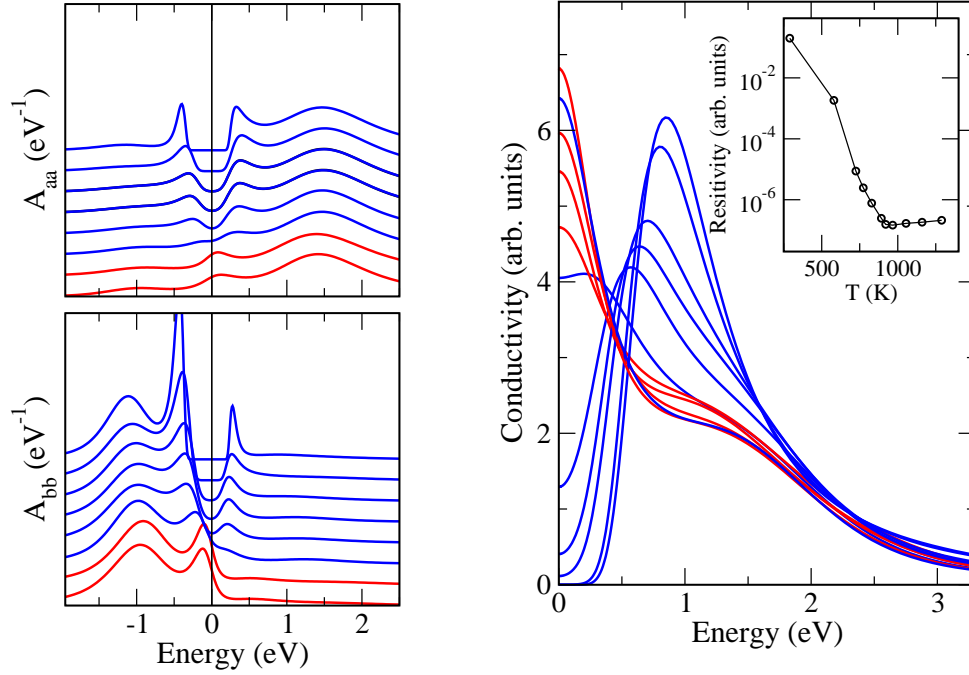


FIG. 3: Left, the evolution of the one-particle spectral function corresponding to a and b orbitals with temperature between 1160 K (bottom) and 290 K (top). Right, the optical conductivity in the same temperature range. In the normal phase (red) the height of the Drude peak increases with decreasing temperature. Lowering the temperature below T_c (blue) leads to suppression of the Drude peak and transfer of the spectral weight to higher energy. The inset shows the evolution of the dc resistivity.

captures the features (i)-(iii) observed in PCCO.

Next, we address the $\text{Pr}^{3+} \rightarrow \text{Pr}^{4+}$ valence transition and the fact that experimental transition is observed in a doped system. An isostructural valence transition points to a near degeneracy of the two charge states of the Pr 4*f* shell, which therefore acts as a charge reservoir keeping the CoO_3 subsystem at a fixed chemical potential rather than fixed particle density. Therefore we have repeated the calculations at fixed chemical potential. In Fig. 2 we show the temperature dependences of the order parameter $|\phi|$ and the particle density n , which reflects the average Pr valence in the real material. Doping the system away from half filling leads to reduction of T_c . While $n(T)$ is almost constant above T_c , below T_c the system draws particles from the reservoir to approach the half filling in a process controlled by gain in the condensation energy and the energy cost of adding electrons. This agrees well with the experimental behavior of the Pr valence⁶. Both in experiment and in the model the average Pr valence changes rapidly, but continuously around T_c . While theoretical $n(T)$ starts growing precisely at T_c its experimental counterpart varies already

at higher temperatures. This is a well-known deficiency of the mean-field theory which lacks the critical fluctuations above T_c . These results show that the Pr valence transition is no coincidence. It is induced by the EC instability to which it provides a positive feedback.

II. LDA+U STUDY

Apart from a quantitative oversimplification, the model calculations neglect the true multi-orbital character of the Co 3d shell and thus neglect possible orbital degeneracy of the EC order parameter. The exchange splitting of the Pr^{4+} ground state, perhaps the most intriguing feature of the low temperature PCCO, is also not captured by the simple model. To overcome these deficiencies we have performed material specific calculations using the density functional LDA+U method, which amounts to a static mean-field solution at zero temperature. The ability of the method to capture complex long-range orders was demonstrated by Cricchio *et al.*^{17,18} on URu_2Si_2 and LaFeAsO .

A. Cubic structure

We start the LDA+U calculations in a hypothetical cubic perovskite structure which allows us to address the symmetry aspects of the problem and provides a starting point for investigation of the lower-symmetry PCCO structure. To ensure the same stoichiometry we put La^{3+} on the A positions occupied by Pr^{4+} and Ca^{2+} in PCCO. To further simplify the problem we did not consider the spin-orbit coupling. The point group of the Hamiltonian is then a product of its orbital and spin components $G = O_h \times SU(2)$. The EC order parameter transforms according to some irreducible representation of G . As in the model calculations, the ferromagnetic Hund's coupling favors the spin part to be an $S = 1$ triplet. The orbital part describes a bound state of e_g -electron and t_{2g} -hole. From $E_g \times T_{2g} = T_{2g} + T_{1g}$ it follows that it transforms either as T_{1g} or T_{2g} representation. Only T_{1g} solutions were found to be stable in the LDA+U calculations. This is understandable considering the shapes of the corresponding excitons. The T_{1g} basis contains $d_{xy} \otimes d_{x^2-y^2}$, $d_{xz} \otimes d_{x^2-z^2}$ and $d_{yz} \otimes d_{y^2-z^2}$ excitons, while the T_{2g} basis consists of $d_{xy} \otimes d_{z^2}$, $d_{xz} \otimes d_{y^2}$ and $d_{zy} \otimes d_{x^2}$. The electron-hole attraction within the T_{1g} exciton is stronger than within the T_{2g} one. More importantly, the electrons and holes forming a T_{1g} exciton have large hopping amplitudes along the same 'in-plane' directions, while the electrons and holes forming a T_{2g} exciton maximize their hopping in perpendicular directions, which is detrimental to the excitonic condensation.

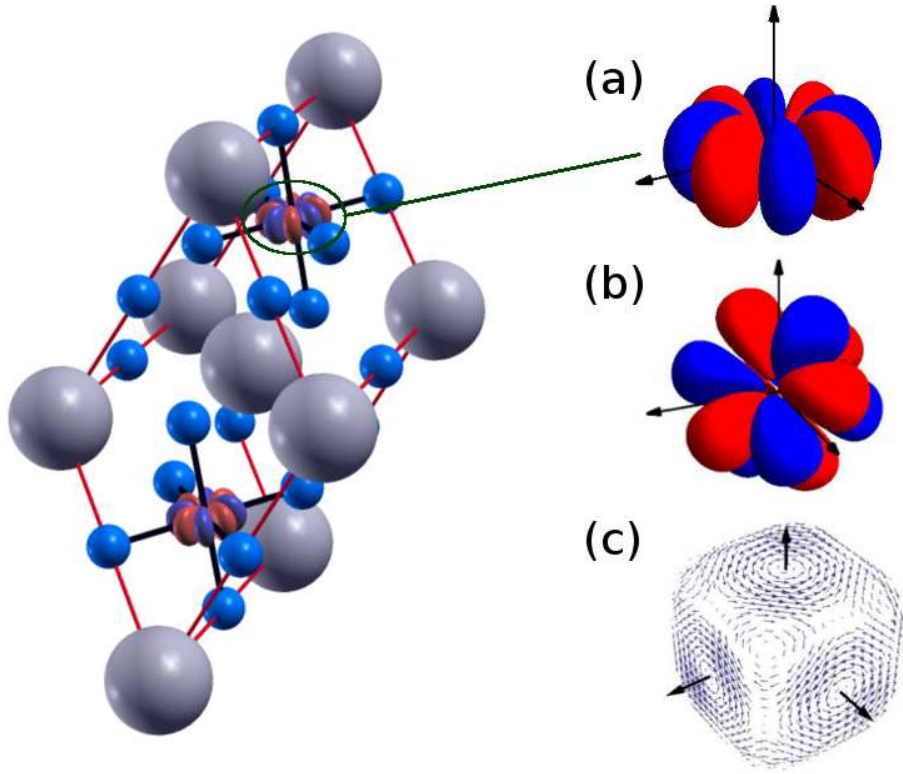


FIG. 4: The rhombohedral unit cell of the cubic structure with spin density depicted as isosurfaces (positive—red, negative—blue) centered on Co sites. The O atoms are blue and La atoms are grey. Details of the spin density around the Co site for three solutions are shown on the right. For product solutions (a) and (b) we use isosurfaces of the collinear spin density. The degenerate solutions can be obtained by O_h operations on the density distribution or continuous rotations of the spin direction. The non-collinear spin distribution of non-product solution (c) is depicted as a tangent vector field on a surface where the normal component vanishes. The transformations to obtain the degenerate solutions are more difficult to visualize, an example is given in Supplementary Figure 2.

The EC order in a cubic crystal is thus characterized by nine parameters ϕ_β^α , where α runs over the three Cartesian spin components and β over three T_{1g} orbital components. In all stable solutions that we found the parameters ϕ_β^α expressed in the above basis were real numbers. The nine component order parameter offers several possible inequivalent solutions, which can be classified by their residual symmetry. All residual symmetries can be obtained by group theoretical methods developed for superfluid He^3 or triplet superconductors^{19,20}. Our goal is not to investigate the stability of all the possible solutions, but to demonstrate the existence of some. The calculations were performed in a rhombohedral unit cell, shown in Fig. 4, which admits ferro and G-type anti-

TABLE I: The orbital parts of the EC order parameter for the four Co atoms the unit cell of PCCO. The local coordinate point approximately along the Co-O bonds. The local coordinates on the pairs of symmetry related Co atoms, 1-2 and 3-4 are connected by σ_h .

	1	2	3	4
ϕ_{yz}	0.182	0.182	0.216	0.216
ϕ_{zx}	0.228	0.228	-0.212	-0.212
ϕ_{xy}	-0.071	0.071	-0.093	0.093

ferro periodicity. Although stable ferro solutions exist, the anti-ferro order was found to have lower energy. Starting from various initial conditions we were able to find three distinct solutions shown in Fig. 4, all of them described by a single parameter X . The order parameter in solutions (a) $\phi_\beta^\alpha = X\delta_{3\beta}\delta_{3\alpha}$ and (b) $\phi_\beta^\alpha = X\delta_{3\alpha}$ is a product of spin and orbital parts and has a continuous residual symmetry. The solution (c) $\phi_\beta^\alpha = X\delta_{\alpha\beta}$ does not have the product form and its discrete residual symmetry group consists of simultaneous spin and orbital operations. Details can be found in the Supplementary Information.

B. PCCO

The calculations on $\text{Pr}_{0.5}\text{Ca}_{0.5}\text{CoO}_3$ were performed in the structure of Ref. 8 with the Pr 4*f* occupancy constrained to 1, corresponding to all Pr atoms being in the 4+ valence state. As in the cubic system we were able to obtain a stable EC solution with energy below that of the normal state. Although the cubic symmetry of the Co sites is only approximate, the anomalous part of the Co 3*d* occupation matrix is dominated by the T_{1g} components when expressed in the local coordinates tied to the CoO_6 octahedra. Compared to the above cubic system, the EC phase in PCCO was more difficult to stabilize. Starting from several different initial conditions the calculations converged to a single product solution shown in Table I and Fig. 5. Importantly for the subsequent discussion, the solution has an odd parity under the mirror image σ_h by a plane perpendicular to the *c*-axis.

Next, we discuss the exchange splitting on the Pr site. Although the spin-orbit coupling is the largest term within the $4f^1$ subspace it is instructive to discuss the situation without it first. The low symmetry crystal-field splits the $4f^1$ subspace into 7 orbital singlets which are either even (A') or odd (A'') under σ_h . In each of the seven states the coupling of the Pr spin to the CoO_3 subsystem can be described by a multi-band Kondo Hamiltonian. Keeping only the local terms that become

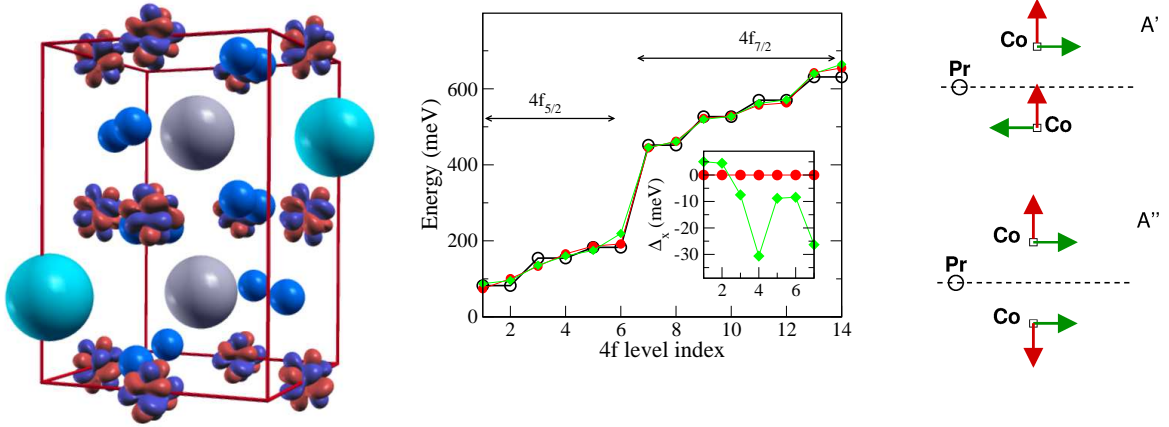


FIG. 5: Left, the collinear spin density around Co atoms in orthorhombic $\text{Pr}_{0.5}\text{Ca}_{0.5}\text{CoO}_3$ with O (blue), Ca (light blue) and Pr (grey). Middle, the energies of the Pr 4f states with spin-orbit coupling: no EC order (black), the order parameter transforms according to A'' representation (red), the order parameter with A' contribution (green). The inset shows the exchange splitting of the 4f levels when spin-orbit coupling is not included. Right, a cartoon picture of the orbital pseudo-vectors on the symmetry related Co atoms transforming according to A' and A'' representations.

c -numbers below T_c we have

$$H^{(n)} = \sum_{\alpha\alpha'} \sum_{mm'} \sum_i \mathbf{S} \cdot \boldsymbol{\sigma}_{\alpha\alpha'} J_{i,mm'}^{(n)} c_{im\alpha}^\dagger c_{im'\alpha'} + \text{c.c.} \quad (1)$$

where \mathbf{S} is Pr spin- $\frac{1}{2}$ operator, $\boldsymbol{\sigma}$ are the Pauli matrices, and $c_{im\alpha}$ is the annihilation operator of an electron with spin index α in a real orbital $|m_i\rangle$ on Co atom i . The coupling constant $J_{i,mm'}^{(n)} \sim \langle m_i | \hat{f} | f^{(n)} \rangle \langle f^{(n)} | \hat{f} | m'_i \rangle$ is proportional to the hopping amplitudes between the orbital $|f^{(n)}\rangle$ of the n th Pr state and the Co orbitals. Although this Hamiltonian is likely to be too simplistic for quantitative calculation it captures the physical mechanism and the symmetry of the problem. The spin-triplet order ensures that below T_c the c operators summed over the spin indices acquire finite expectation value and give rise to an effective exchange field

$$h_\gamma^{(n)} = \sum_{imm'} J_{i,mm'}^{(n)} \sum_{\alpha\alpha'} 2 \text{Re} \langle c_{im\alpha}^\dagger \sigma_{\alpha\alpha'}^\gamma c_{im'\alpha'} \rangle, \quad (2)$$

where we have used the fact that $J_{i,mm'}^{(n)}$ is real in the basis of real orbitals. In order to establish that $h_\gamma^{(n)}$ is not zero due to destructive interference of coupling to different Co atoms we have to consider the transformation properties of $|f^{(n)}\rangle \langle f^{(n)}|$ and $\sum_i |m'_i\rangle \langle c_{im\alpha}^\dagger c_{im'\alpha'} \rangle \langle m_i|$ under the point group of the Pr site, which contains only identity and σ_h . The possible symmetries of the latter are depicted in Fig. 5 using the fact that the T_{1g} order parameter transforms as a pseudo-vector

under orbital transformations. The calculated order parameter belongs to the A'' representation and therefore does not couple to any of the $4f$ states since $|f^{(n)}\rangle\langle f^{(n)}|$ transforms according to the A' representation for all n 's. This is confirmed by the results of a direct numerical calculation of the Pr exchange splitting. For comparison we have calculated the exchange splitting induced by an artificial order parameter of the same magnitude containing a non-zero A' component.²⁹ Both results are shown in the inset of Fig. 5.

Taking into account the strong spin-orbit coupling on the Pr site changes the picture substantially. While it preserves the spectrum of seven Kramers doublets it mixes the A' and A'' orbital components in the eigenstates $|f^{(n)}\rangle$. The product $|f^{(n)}\rangle\langle f^{(n)}|$ therefore contains both A' and A'' contributions and couple to the EC order parameter of A'' symmetry as well. The exchange split $4f$ spectra, obtained in an LDA+U calculation described in the Methods section, are shown in Fig. 5. The exchange splitting of the order of 10 meV overestimates the experimental values of a few Kelvin. This is not surprising given the approximations involved, in particular the mean-field treatment of the Pr $4f$ shell which in reality presents a complicated quantum impurity problem.

III. SUMMARY

Excitonic condensation provides a comprehensive description of the phase transition observed in the PCCO series. While some of the points (i)-(iv) taken alone admit more conventional explanations, such as spin-state crossover, we are not aware of a reliable alternative theory describing the exchange splitting of the Pr $4f$ states. It is not clear at the moment why the excitonic condensation takes place in PCCO, but not in other cobaltites close to stoichiometric filling, e.g. LaCoO_3 . The answer may be related to whether the lowest excited state of the Co ion has total spin $S = 2$ or $S = 1$. The $S = 2$ site tend to form a solid lattice on the LS background^{14,21}, while $S = 1$ states are susceptible to the present condensation. Resolving this question is beyond the scope of the present work.

The low-temperature phase of PCCO is an example of complex multipole order which is detected only through its indirect effects. Unlike URu_2Si_2 or LaOFeAs where the hidden order and nematicity arise from Fermi surface nesting^{22,23}, PCCO are correlated oxides and the transition here is closer to condensation of preexisting composite bosons. The present mechanism of the excitonic condensation is quite general and therefore it should be possible to find it in other materials exhibiting singlet-triplet spin-state transitions.²⁴

IV. METHODS

A. Model calculation

The DMFT calculations were performed for the two-band Hubbard model with nearest-neighbor (nn) hopping on a bipartite (square) lattice and density-density interaction

$$\begin{aligned}
H = & \mu \sum_{i,\alpha} (n_{i\alpha}^a + n_{i\alpha}^b) + \frac{\Delta}{2} \sum_{i,\alpha} (n_{i\alpha}^a - n_{i\alpha}^b) + \sum_{i,j,\alpha} (t_a a_{i\alpha}^\dagger a_{j\alpha} + t_b b_{i\alpha}^\dagger b_{j\alpha}) \\
& + U \sum_i (n_{i\uparrow}^a n_{i\downarrow}^a + n_{i\uparrow}^b n_{i\downarrow}^b) + (U - 2J) \sum_{i,\alpha} n_{i\alpha}^a n_{i-\alpha}^b + (U - 3J) \sum_{i\alpha} n_{i\alpha}^a n_{i\alpha}^b.
\end{aligned} \tag{3}$$

Here $a_{i\alpha}^\dagger$, $b_{i\alpha}^\dagger$ are the creation operators of fermions with spin $\alpha = \uparrow, \downarrow$ on the lattice site i and $n_{i\alpha}^c = c_{i\alpha}^\dagger c_{i\alpha}$ are the corresponding occupation number operators. The calculations were performed for $U = 4$, $J = 1$, $t_a = 0.4118$, $t_b = -0.1882$ and $\Delta = 3.40$, assuming eV the unit of energy and expressing the temperatures in Kelvin. We use the continuous-time quantum Monte-Carlo impurity solver of Werner *et al.*²⁵, which we modified to treat off-diagonal terms in the hybridization function. We used TRIQS implementation of the continuous-time quantum Monte-Carlo as a benchmark and in all tested cases obtained identical results within the computational accuracy. The spectral functions were obtained with the maximum entropy methods²⁶ applied to the local Green's functions. The optical conductivities were calculated on the Matsubara contour and analytically continued to the real frequencies using the maximum entropy method. The vertex corrections were not considered. The spin susceptibility was calculated as $\Delta M / \Delta h$ in a finite field of 0.001 eV/ μ_B . We have checked the linearity of M vs h for several parameters and compared the susceptibilities in the normal phase to the linear response values¹¹ finding an agreement within the error bars.

B. LDA+U

The LDA+U calculations were performed with Wien2k²⁷ package. No symmetries were enforced on the system to allow the broken symmetry solutions. Spin-orbit coupling was switched off. Calculations both with LDA+U (only charge density is used to compute the exchange-correlation potential) and with LSDA+U (the spin and charge densities are used to compute spin-dependent exchange-correlation potential) were performed with the result that LSDA+U leads to somewhat larger condensation energies, i.e. more stable EC phase. LSDA+U calculations were restricted to collinear spin densities (order parameters of product form). The Pr 4f's were treated as core

states with occupancy of 1 in the self-consistent calculations. To obtain the exchange splitting on Pr the effective LDA+U Hamiltonian was diagonalized with the $4f$'s in the valence basis. We used an orbital potential to locate the $4f$ levels inside the gap close to the chemical potential in order to mimick the charge transfer energy corresponding to $4f^1 \rightarrow 4f^2\bar{L}$ process, which we assume to constitute the largest contribution to $J_{i,mm'}^{(n)}$.

* Electronic address: kunes@fzu.cz

- ¹ Tsubouchi, S. *et al.* Simultaneous metal-insulator and spin-state transitions in $\text{Pr}_{0.5}\text{Ca}_{0.5}\text{CoO}_3$. *Phys. Rev. B* **66**, 052418 (2002).
- ² Tsubouchi, S., Kyômen, T., Itoh, M. & Oguni, M. Electric, magnetic, and calorimetric properties and phase diagram of $\text{Pr}_{1-x}\text{Ca}_x\text{CoO}_3$ ($0 \leq x \leq 0.55$). *Phys. Rev. B* **69**, 144406 (2004).
- ³ Fujita, T. *et al.* Transport and magnetic studies on the spin state transition of $\text{Pr}_{1-x}\text{Ca}_x\text{CoO}_3$ up to high pressure. *Journal of the Physical Society of Japan* **73**, 1987–1997 (2004).
- ⁴ Hejtmánek, J. *et al.* Metal-insulator transition and the $\text{Pr}^{3+}/\text{Pr}^{4+}$ valence shift in $(\text{Pr}_{1-y}\text{Y}_y)_{0.7}\text{Ca}_{0.3}\text{CoO}_3$. *Phys. Rev. B* **82**, 165107 (2010).
- ⁵ Hardy, V., Guillou, F. & Brard, Y. Jumps in entropy and magnetic susceptibility at the valence and spin-state transition in a cobalt oxide. *Journal of Physics: Condensed Matter* **25**, 246003 (2013).
- ⁶ Hejtmánek, J. *et al.* Phase transition in $\text{Pr}_{0.5}\text{Ca}_{0.5}\text{CoO}_3$ and related cobaltites. *The European Physical Journal B* **86**, 1–8 (2013).
- ⁷ Mydosh, J. A. & Oppeneer, P. M. Colloquium: Hidden order, superconductivity, and magnetism: The unsolved case of URu_2Si_2 . *Rev. Mod. Phys.* **83**, 1301–1322 (2011).
- ⁸ Knížek, K., Hejtmánek, J., Novák, P. & Jiráček, Z. Charge transfer, valence, and the metal-insulator transition in $\text{Pr}_{0.5}\text{Ca}_{0.5}\text{CoO}_3$. *Phys. Rev. B* **81**, 155113 (2010).
- ⁹ Knížek, K. *et al.* Spin-state crossover and low-temperature magnetic state in yttrium-doped $\text{Pr}_{0.7}\text{Ca}_{0.3}\text{CoO}_3$. *Phys. Rev. B* **88**, 224412 (2013).
- ¹⁰ Herrero-Martín, J. *et al.* Spin-state transition in $\text{Pr}_{0.5}\text{Ca}_{0.5}\text{CoO}_3$ analyzed by x-ray absorption and emission spectroscopies. *Phys. Rev. B* **86**, 125106 (2012).
- ¹¹ Kuneš, J. & Augustinský, P. Excitonic instability at the spin-state transition in the two-band Hubbard model. *Phys. Rev. B* **89**, 115134 (2014).
- ¹² Shick, A. B., Liechtenstein, A. I. & Pickett, W. E. Implementation of the LDA+U method using the full-potential linearized augmented plane-wave basis. *Phys. Rev. B* **60**, 10763–10769 (1999).
- ¹³ Werner, P. & Millis, A. J. High-spin to low-spin and orbital polarization transitions in multiorbital Mott systems. *Phys. Rev. Lett.* **99**, 126405 (2007).
- ¹⁴ Kuneš, J. & Křápek, V. Disproportionation and metallization at low-spin to high-spin transition in

- multiorbital Mott systems. *Phys. Rev. Lett.* **106**, 256401 (2011).
- ¹⁵ Halperin, B. I. & Rice, T. M. Possible anomalies at a semimetal-semiconductor transition. *Rev. Mod. Phys.* **40**, 755–766 (1968).
- ¹⁶ Batista, C. D. Electronic ferroelectricity in the Falicov-Kimball model. *Phys. Rev. Lett.* **89**, 166403 (2002).
- ¹⁷ Cricchio, F., Bultmark, F., Grånäs, O. & Nordström, L. Itinerant magnetic multipole moments of rank five as the hidden order in URu₂Si₂. *Phys. Rev. Lett.* **103**, 107202 (2009).
- ¹⁸ Cricchio, F., Grånäs, O. & Nordström, L. Low spin moment due to hidden multipole order from spin-orbital ordering in LaFeAsO. *Phys. Rev. B* **81**, 140403 (2010).
- ¹⁹ Bruder, C. & Vollhardt, D. Symmetry and stationary points of a free energy: The case of superfluid ³He. *Phys. Rev. B* **34**, 131–146 (1986).
- ²⁰ Annett, J. F. Symmetry of the order parameter for high-temperature superconductivity. *Adv. Phys.* **39**, 83 (1990).
- ²¹ Knížek, K., Jiráček, Z., Hejtmánek, J., Novák, P. & Ku, W. GGA+U calculations of correlated spin excitations in LaCoO₃. *Phys. Rev. B* **79**, 014430 (2009).
- ²² Ikeda, H. *et al.* Emergent rank-5 nematic order in URu₂Si₂. *Nat. Phys.* **8**, 528 (2012).
- ²³ Fernandes, R. M., Chubukov, A. V. & Schmalian, J. What drives nematic order in iron-based superconductors? *Nat. Phys.* **10**, 97 (2014).
- ²⁴ Khaliullin, G. Excitonic magnetism in Van Vleck-type d⁴ Mott insulators. *Phys. Rev. Lett.* **111**, 197201 (2013).
- ²⁵ Werner, P., Comanac, A., de’ Medici, L., Troyer, M. & Millis, A. J. Continuous-time solver for quantum impurity models. *Phys. Rev. Lett.* **97**, 076405 (2006).
- ²⁶ Gubernatis, J. E., Jarrell, M., Silver, R. N. & Sivia, D. S. Quantum monte carlo simulations and maximum entropy: Dynamics from imaginary-time data. *Phys. Rev. B* **44**, 6011–6029 (1991).
- ²⁷ Blaha, P., Schwarz, K., Madsen, G. K. H., Kvasnicka, D. & Luitz, J. *WIEN2K, An Augmented Plane Wave + Local Orbitals Program for Calculating Crystal Properties* (Karlheinz Schwarz, Techn. Universität Wien, Austria, 2001).
- ²⁸ There is another degeneracy with respect the phase of ϕ connected to the conservation of each orbital flavor separately. This is a non-generic feature specific to our simple model, which is not present in real materials
- ²⁹ obtained by changing the sign of ϕ_{zx} on one of the two symmetry related Co atoms

Acknowledgments

We acknowledge numerous discussions with Z. Jirák, P. Novák, A. Kauch and D. Vollhardt. The work was supported through the research unit FOR 1346 of the Deutsche Forschungsgemeinschaft and the grant 13-25251S of the Grant Agency of the Czech Republic.

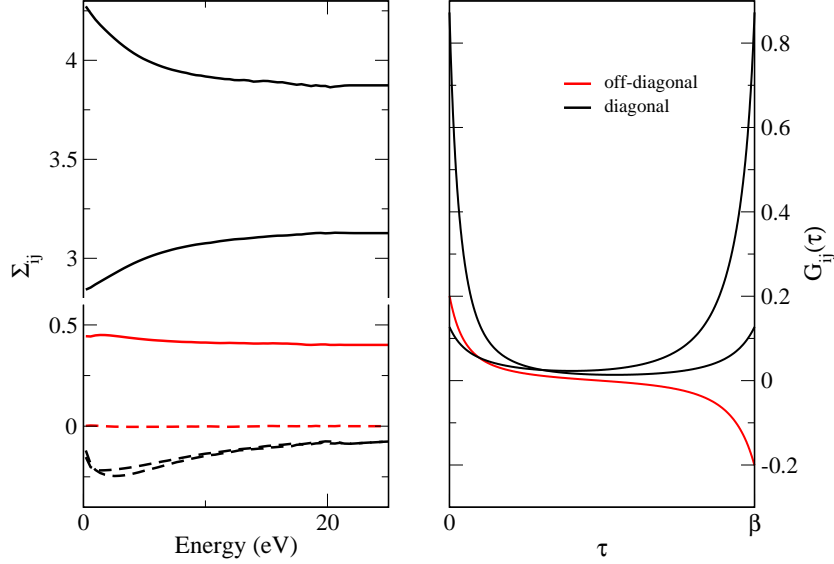


FIG. 6: Left, the self-energy $\Sigma_{ij}(\omega_n)$ of the half-filled model at $T=725$ K on the Matsubara contour. The real and imaginary parts are marked with full and dashed lines, respectively. Right, the corresponding local Green's function $G_{ij}(\tau)$ at the imaginary times.

V. SUPPLEMENTARY INFORMATION

A. DMFT

In Fig. 6 we show an example of a typical self-energy $\Sigma(i\omega_n)$ and the local Green's function $G(\tau)$ in the EC phase. The non-zero diagonal elements correspond to orbital-spin pairs $a\sigma, a\sigma$ and $b\sigma, b\sigma$ with $\sigma = \uparrow, \downarrow$. The non-zero off-diagonal correspond to $a\sigma, b - \sigma$ and $b\sigma, a - \sigma$.

B. LDA+U results in cubic perovskite structure

The LDA+U calculations were performed in a cubic perovskite structure with La on the A position and the lattice parameter of 5.4347 Å. We used the Wien2k package with the around mean-field double counting correction. The '+U' orbital potential was added for the Co 3d shell. In order to include the spin off-diagonal elements of the orbital potential we used the LAPWSO code, but switched spin-orbit potential on all atoms off.

The EC order parameter can be obtained from the on-site occupation matrix of the Co 3d shell

$D_{mm',ss'} = \langle c_{ms}^\dagger c_{m's'} \rangle$, where m is the orbital and s the spin index. In general, the symmetry dictates the EC pairing function to be an irreducible representation of the symmetry group of the system. The ferromagnetic Hund's coupling and the band filling restricts possible pairing functions to spin-triplets and orbital $E_g \times T_{2g} = T_{1g} + T_{2g}$ irreducible representations, out of which the T_{1g} is favorable for reasons given in the main text and verified by direct computation. The spin structure of the occupation matrix \mathbf{D} in the ordered phase reads

$$\mathbf{D} = \begin{pmatrix} \mathbf{D}_0 + \phi^z & \phi^x + i\phi^y \\ (\phi^x + i\phi^y)^* & \mathbf{D}_0 - \phi^z \end{pmatrix}, \quad (4)$$

where the normal part \mathbf{D}_0 and the anomalous parts ϕ^α are 5×5 matrices in the orbital space. The orbital part of ϕ^α can be written as a linear combination of the T_{1g} basis functions $\phi^\alpha = \phi_{xy}^\alpha d_{x^2-y^2} \otimes d_{xy} + \phi_{zx}^\alpha d_{z^2-x^2} \otimes d_{zx} + \phi_{yz}^\alpha d_{y^2-z^2} \otimes d_{yz}$. The EC phase is thus characterized by 9-component order parameter ϕ_β^α . The order parameter ϕ_β^α can have some phase freedom in case that some orbital flavors are conserved, as is the case when only nearest neighbor hopping is considered. In real materials the orbital flavors are typically not conserved and thus the phases of ϕ_β^α are fixed. In all presented calculations we found ϕ_β^α to be real.

Expressed in the spherical harmonic basis of Wien2k the orbital matrices take the form

$$\phi' = \begin{pmatrix} 0 & -\frac{1}{4}(\phi'_{zx} + i\phi'_{yz}) & 0 & \frac{1}{4}(\phi'_{zx} - i\phi'_{yz}) & i\phi'_{xy} \\ -\frac{1}{4}(\phi'_{zx} - i\phi'_{yz}) & 0 & \sqrt{\frac{3}{8}}(\phi'_{zx} + i\phi'_{yz}) & 0 & -\frac{1}{4}(\phi'_{zx} - i\phi'_{yz}) \\ 0 & \sqrt{\frac{3}{8}}(\phi'_{zx} - i\phi'_{yz}) & 0 & -\sqrt{\frac{3}{8}}(\phi'_{zx} + i\phi'_{yz}) & 0 \\ \frac{1}{4}(\phi'_{zx} + i\phi'_{yz}) & 0 & -\sqrt{\frac{3}{8}}(\phi'_{zx} - i\phi'_{yz}) & 0 & \frac{1}{4}(\phi'_{zx} + i\phi'_{yz}) \\ -i\phi'_{xy} & -\frac{1}{4}(\phi'_{zx} + i\phi'_{yz}) & 0 & \frac{1}{4}(\phi'_{zx} - i\phi'_{yz}) & 0 \end{pmatrix}$$

$$\phi'' = \begin{pmatrix} \phi''_{xy} & -\frac{1}{4}(i\phi''_{zx} - \phi''_{yz}) & 0 & \frac{1}{4}(i\phi''_{zx} + \phi''_{yz}) & 0 \\ \frac{1}{4}(i\phi''_{zx} + \phi''_{yz}) & 0 & -\sqrt{\frac{3}{8}}(i\phi''_{zx} - \phi''_{yz}) & 0 & \frac{1}{4}(i\phi''_{zx} + \phi''_{yz}) \\ 0 & \sqrt{\frac{3}{8}}(i\phi''_{zx} + \phi''_{yz}) & 0 & -\sqrt{\frac{3}{8}}(i\phi''_{zx} - \phi''_{yz}) & 0 \\ -\frac{1}{4}(i\phi''_{zx} - \phi''_{yz}) & 0 & \sqrt{\frac{3}{8}}(i\phi''_{zx} + \phi''_{yz}) & 0 & -\frac{1}{4}(i\phi''_{zx} - \phi''_{yz}) \\ 0 & -\frac{1}{4}(i\phi''_{zx} - \phi''_{yz}) & 0 & \frac{1}{4}(i\phi''_{zx} + \phi''_{yz}) & -\phi''_{xy} \end{pmatrix},$$

where we have dropped the index α and separate the real and imaginary parts in $\phi = \phi' + i\phi''$.

The ordered phase is characterized by its residual symmetry. A complete list of possible phases with T_{1g} triplet pairing can be obtained by group theoretical methods in analogy to studies of He^3 or triplet superconductors. It is not our goal to investigate the stability of all the possible

phases. We want to provide examples of several stable solution with EC order to demonstrate the feasibility of such state in cobaltites. We start with phases where the orbital and spin parts of the order parameter factorize, $\phi_\beta^\alpha = o_\beta \otimes s^\alpha$. We found two such solutions. The first solution

$$\phi_{(1)} = \begin{pmatrix} 0 & 0 & X \\ 0 & 0 & 0 \\ 0 & 0 & 0 \end{pmatrix}, \quad \begin{pmatrix} 0 & 0 & 0 \\ 0 & 0 & X \\ 0 & 0 & 0 \end{pmatrix}, \quad \begin{pmatrix} X \cos(\gamma) & X \sin(\gamma) & 0 \\ 0 & 0 & 0 \\ 0 & 0 & 0 \end{pmatrix}. \quad (5)$$

with the residual symmetry $\tilde{D}_{4h} \times U(1)$, where the group $\tilde{D}_{4h} = \{C_{4h}, \sigma_v C_{4h} \times c_2\}$ contains the elements of C_{4h} , which keep the orbital part unchanged, and the element of D_{4h} which change the sign of the orbital part coupled to π -rotation in the spin space about an axis perpendicular the $U(1)$ axis. We have constructed several equivalent solutions listed above related by an arbitrary spin rotation or an O_h rotation the orbital space. We have verified that these solutions yield the same amplitudes of the order parameter, total energies and the one-particle densities of states. As a technical side remark we point out that to ensure these symmetry properties with Wien2k the calculations must be performed in LDA+U and not LSDA+U mode. We have found that feeding the spin density into the exchange-correlation functional (as done in LSDA+U) enhances the EC order. However, this type of calculation with the spin-collinear Wien2k code breaks by construction the spin rotational symmetry.

The second solution we have found for the order parameter

$$\phi_{(2)} = \begin{pmatrix} 0 & 0 & X \\ 0 & 0 & X \\ 0 & 0 & X \end{pmatrix}, \quad (6)$$

with the residual symmetry $\tilde{D}_{3d} \times U(1)$, where the tilde again means that operations which change the sign of the orbital part are coupled to a π -rotation in the spin space. Calculations starting from arbitrary orbital always converged to one of these solutions.

Finally, we have found a non-product solution, which has only discrete residual symmetry isomorphic to O_h , with the order parameter

$$\phi_{(3)} = \begin{pmatrix} X & 0 & 0 \\ 0 & X & 0 \\ 0 & 0 & X \end{pmatrix}. \quad (7)$$

The residual symmetry group contains the O_h element, which transform the orbital part as proper rotations, coupled to the corresponding spin rotation and the O_h elements, which transform the

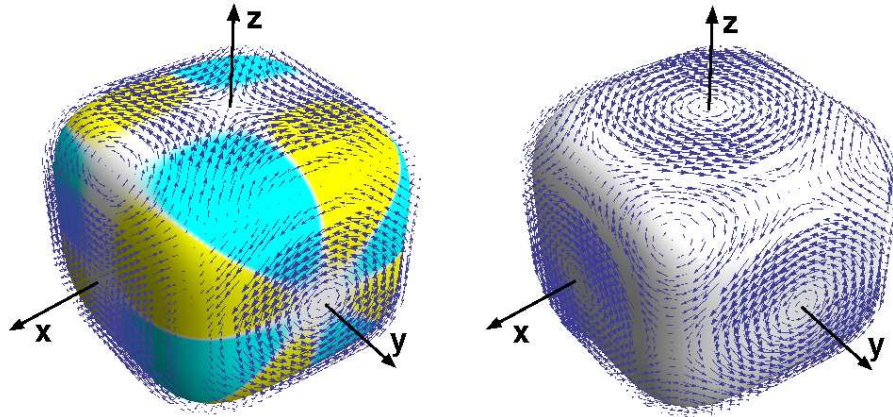


FIG. 7: The spin density distribution on a $x^4 + y^4 + z^4 = \text{const}$ surface around a Co atom for the non-product solution (7) (right) and another degenerate solution obtained by $\phi_2^2 \leftrightarrow -\phi_2^2$ (left). The color codes the normal component (white stands for 0, yellow and blue for positive and negative values, respectively) while the tangent component is depicted by arrows.

orbital part as improper rotations, coupled to the spin rotation and the time reversal. In Fig. 7 we show two examples of degenerate non-product solutions.

C. LDA+U in PCCO structure

The calculations on $\text{Pr}_{0.5}\text{Ca}_{0.5}\text{CoO}_3$ were performed in the orthorhombic structure with regular rock-salt arrangement of Pr and Ca atoms and four formula units in the unit cell. The Pr $4f$ states were treated as core state and their number was constrained to 1 per atom. We used the same interaction parameters as in the cubic LaCoO_3 . Since the cubic symmetry of Co sites in PCCO is broken in this system the T_{1g} symmetry of the pairing function is only approximate. Nevertheless, projection onto the T_{1g} pairing orbitals with respect to the coordinates tied to the local CoO_6 octahedron for each Co atom contains about 90% of the anomalous parts of the occupation matrices (measured by $\sum_{ij} |D_{ij}|^2$). Therefore one can still use the order parameter ϕ_β^α to provide the first approximation of the ordered state.

In the PCCO calculations we have searched only ferro states of the product form (note the above AF periodicity fits as ferro state into the larger unit cell of PCCO). Such states are completely described by the orbital part on each of the four Co atoms in the unit cell. Starting from several

TABLE II: The amplitudes of the order parameter and the LDA+U total energies relative to the normal states for several AF EC orders.

i	X	$E_{(i)}$ [meV/f.u.]
1	0.182	-43
2	0.134	-73
3	0.144	-82

TABLE III: The orbital parts of the EC order parameter for the four Co atoms the unit cell of PCCO. The spin part is an arbitrary unit vector (the actual calculations were performed with \mathbf{e}_z). The local coordinates were chosen such that the corresponding axes on different Co atoms are approximately parallel. The last line shows the magnetic moment inside the Wien2k atomic spheres.

	1	2	3	4
ϕ_{yz}	0.182	0.182	0.216	0.216
ϕ_{zx}	0.228	0.228	-0.212	-0.212
ϕ_{xy}	-0.071	0.071	-0.093	0.093
m_z [μ_B]	-0.014	0.014	0.023	-0.023

initial conditions we found one stable solution with the order parameter given in table III. The EC order causes finite spin density distribution in the crystal. Because of the low-symmetry of the structure this leads to a small moments appearing when integrated over the Wien2k atomic spheres (shown in Table III). Given their small size we do not assign much significance to the actual numbers, which depend the non-physical parameter the sphere radius. More importantly we observe that the total moment per unit cell is zero up to the computational accuracy.